Propulsion and Energy Forum
July 28-30, 2014, Cleveland, OH
50th AIAA/ASME/SAE/ASEE Joint Propulsion Conference

Effect of Fin-Guided Fuel Injection on Dual Mode Scramjet Operation

Camilo Aguilera* and Ken H. Yu†
University of Maryland, College Park, Maryland 20742

Supersonic combustion experiments were conducted to determine the effects of using a mixing enhancement fin on dual mode scramjet operation. This fin-guided injection approach was compared against a baseline where no fin was used. A direct-connect vitiated air facility was used to simulate the total enthalpy of a Mach 4.6 flight condition and generated a Mach 2 flow at the isolator inlet. The laboratory scale tests were performed in a model combustor designed with a cavity flameholder and a 2º expansion. The experiments used hydrogen fuel at an overall equivalence ratio ranging between 0.04-0.19. The combustor flowfield was qualitatively analyzed using schlieren visualizations and *OH chemiluminescence, while more quantitative assessments were made by comparing combustor wall pressure distributions. The results showed that the combustor operated in scramjet mode only at relatively low equivalence ratios and became thermally choked at higher equivalence ratios. With the use of the fin, the upper limit of supersonic combustion was extended to an equivalence ratio of 0.12 from 0.08 for the baseline case by preventing thermal choking caused by concentrated heat release near the cavity and the combustor wall. Increased fuel penetration afforded by the fin was responsible for this result by displacing the flame away from the cavity wall to the expanding section of the supersonic core flow and by stretching the reaction zone axially. This would be advantageous for reducing heat transfer to the wall but it also made the cavity flameholder less effective and the flame length longer.**

Nomenclature

∞	=	Freestream Condition
2	=	Isolator Entrance
$\dot{m}$	=	Mass Flow Rate
Φ	=	Equivalence Ratio
D	=	Injector Orifice Diameter
*h**	=	Throat Height (~ 6.9 mm, ~ 0.27 in)
H	=	Isolator Height (12.7 mm, 0.5 in) or Hydrogen Atom
*OH**	=	Excited Hydroxyl Radical
O, M	=	Oxygen Atom, Third Body Collider
I	=	*OH** Signal Intensity
P	=	Pressure
P0	=	Stagnation Pressure
T	=	Temperature
T0	=	Stagnation Temperature
x	=	Axial Coordinate
comb	=	Combustor
HD	=	Hydraulic Diameter
IG	=	Igniter
vit	=	Vitiated

*Research Associate, Aerospace Engineering Department, 2104A Glenn L. Martin Wind Tunnel Building, University of Maryland, College Park, AIAA Member.
†Associate Professor, Aerospace Engineering Department, 3152 Glenn L. Martin Hall, University of Maryland, College Park, AIAA Associate Fellow.

I. Introduction

ACHIEVING efficient fuel-air mixing is a preeminent problem in a supersonic combustor due to the compressibility effect[1-9] on the mixing shear layer growth and the stringent flow residence time limitation imposed by the high speed crossflow. A considerable amount of research has therefore been done on mixing enhancement techniques involving injector design with the goal of increasing mixing over a wide range of flow length scales[10-13] in an effort to improve combustion efficiency. Among those, a wall circular orifice is considered the simplest approach to scramjet fuel injection and has been thoroughly studied[14-16]. This injection configuration has very well understood mixing mechanisms that can shorten combustor lengths compared to other injection strategies like parallel injection[17]. However, it requires a high momentum jet to provide adequate fuel penetration, which is key to enhance mixing and provide uniform fuel delivery into a low aspect ratio combustor.

Jet-induced shocks generated by fuel injection from a wall in a supersonic combustor can cause a significant free stream stagnation pressure loss when the jet momentum and the flow Mach number are high. These pressure losses lead to undesirable thrust performance penalties that should be minimized. One approach to mitigate jet-induced shock losses is to mount a thin triangular-shaped pylon or fin upstream of the wall injection orifice. The word "fin" is used to underline the slender dimension of its base width designed to equal the injector diameter and avoid any additional flow blockage to what would be naturally incurred with a transverse jet. In earlier non-reacting studies, this injection strategy allowed increasing fuel penetration by 100-200% without increasing jet momentum in comparison to the baseline with a 33-47% shock strength reduction[18]. However, insight into the potential effect of increased jet penetration achieved with this fin on scramjet performance requires investigating fin-guided injection in a reacting flow environment.

This study is therefore a continuation of previous mixing experiments with the main goal of investigating and comparing the combustion operation of a dual mode scramjet using conventional transverse wall injection (baseline) and its modified fin-guided alternative. A set of experiments were conducted for this purpose with the same fin design studied earlier but a new supersonic flow path with a cavity flameholder and an expanding section.

II. Experimental Setup

A. Direct-Connect Facility

The scramjet fuel injection experiments performed were completed using a direct-connect hydrogen-vitiated heater at the Propulsion Research Laboratory at the University of Maryland. Figure 1 shows a schematic of the flow path through this three component facility capable of matching the total enthalpy conditions expected for a vehicle flying at Mach 4.6 at an altitude of ~19 km. An Atlas Copco GA 75 Type compressor connected in series to a Hankison HPRP 400-460 dryer were used to deliver high pressure air for the experiments. The dry airflow entered the facility through a 10.16 mm (0.4 in) orifice used as an acoustic boundary and flow measuring device. Downstream of this orifice, air travelled through an expansion joint, a blow out port section, and an expansion coupler that widened the flow path from a 52.5 mm (2.067 in) diameter circular section to a 77.9 mm (3.068 in) one.

The fuel delivery, mixing, and ignition systems used in this heater were inspired by the typical gas turbine combustor design. A fuel delivery pipe was connected to an industrial gas mixer installed inside a liner cone. Flow

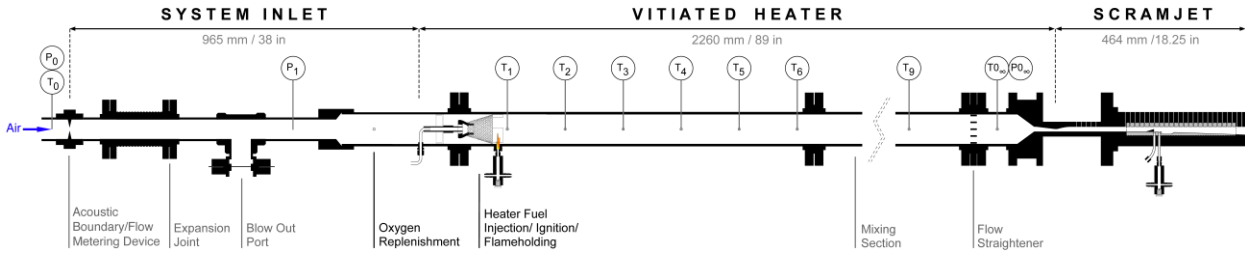

Figure 1. Schematic of the direct-connect facility flow path through its three main components: inlet, vitiated heater, and scramjet. Diagram drawn to scale.

ignition was achieved with an igniter placed just downstream of the liner cone that used an Autolite Copper Core Spark Plug driven by an AC Delco D585 ignition coil. A long section composed of three separate and custom made 304 stainless steel pipes was then used to contain the hydrogen flame.

Oxygen replenishment was performed through two side ports located upstream of the heater main fuel injection location to preserve the atmospheric oxygen mole fraction content of the flow entering the supersonic combustor. A 304 stainless steel machined flow straightener was used near the exit of the heater, upstream of a custom made circular to square transition section used to connect the scramjet. Stagnation pressure measurements ($P0_\infty$) were gathered upstream of the flow path reduction using a Setra 206 transducer. Flow temperature profiles were also obtained at this location by traversing a K-type thermocouple and gathering measurements at various radial locations. The profiles obtained were used to calculate a bulk stagnation temperature value ($T0_\infty$) used to reference the flight condition simulated. Table 1 summarizes some of the main average operating parameters of the vitiated air heater used.

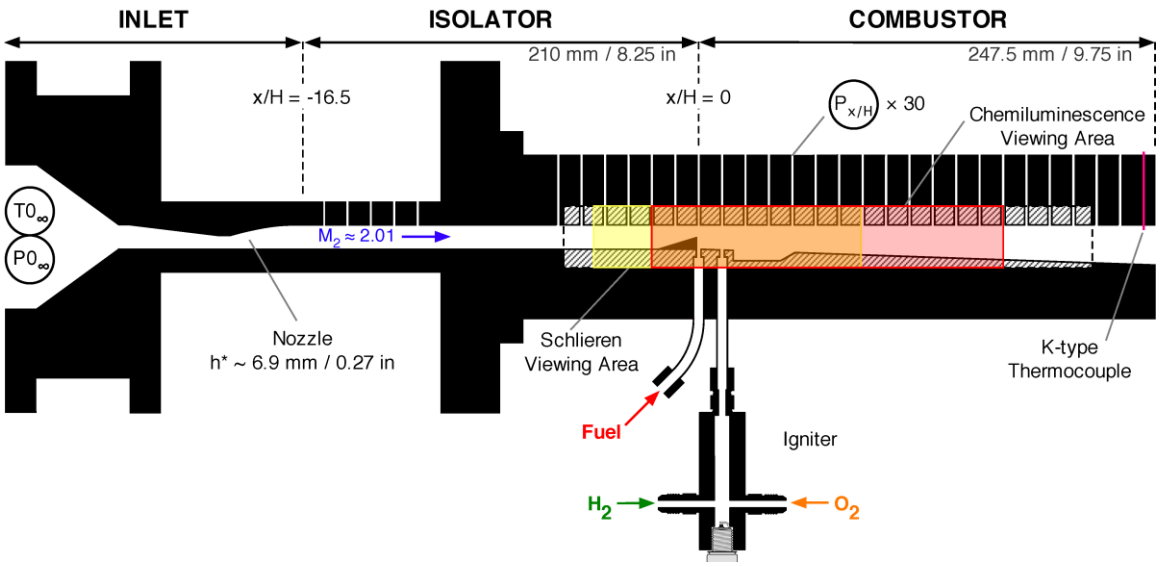

Figure 2. Schematic of isolator side cross section and combustor flow path. The hashed region highlights the location of a quartz window for visual access. Regions of interest for imaging diagnostics and location of pressure ports along the flow path are also shown.

Figure 2 shows a schematic of the supersonic flow path connected to the vitiated heater and Table 2 summarizes the conditions of the high enthalpy flow downstream of the supersonic nozzle based on static pressure measurements and the values of $P0_\infty$ and $T0_\infty$. The isolator section flow path was a constant area duct with a square cross section and a 12.7 mm (0.5 in) duct height, H. At the combustor inlet ($x/H = 0$), a circular 2.4 mm (0.08 in) diameter D wall orifice was used for transverse fuel injection. Downstream of this point, the bottom wall expanded at a 2° rate to alleviate the pressure rise expected due to combustion.

Table 1. Heater flow average operating conditions.

Property	Value	Unit
Stagnation Temperature, $T0_\infty$	1110 ± 20	*K*
Stagnation Pressure, $P0_\infty$	6.68 ± 0.04	*atm*
Flight Mach Simulated, M_∞	4.56 ± 0.05	-
Flight Altitude Simulated, Z_∞	18.9 ± 0.01	*km*

Table 2. Isolator flow typical inlet conditions.

Property	Value	Unit
Mach Number, M_2	2	-
Static Pressure, P_2	0.87	*atm*
Flow Velocity, u_2	1065	*m/s*
$Re_{HD,2}$	1.14×10^5	-

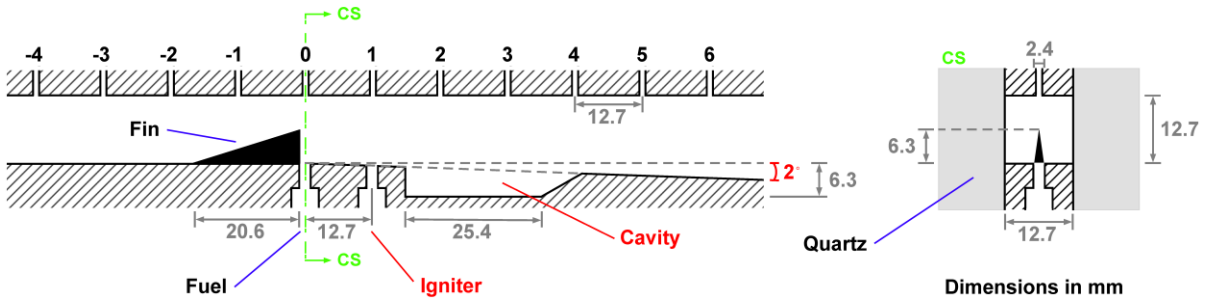

Figure 3. Test section detail showing fin-guided injection configuration, igniter location, cavity geometry, duct expansion, and key dimensions.

Figure 3 shows a detailed view of the test section with the fin-guided configuration. A second orifice with a diameter *D* was drilled *1H* downstream of the main injection orifice and used to inject hot combustion products to ignite the main flow. The geometry and specific location of the cavity flameholder used are also shown and were based on the work done by Yu et. al.[13] The design of the fin was a scaled down version of a previously tested geometry[18] and was placed just upstream of the fuel injection orifice. The resulting displacement in the flow path cross-sectional area caused by this fin was equivalent to the displacement of a 1.4° ramp if the entire span of the duct is considered. Two *1H* thick quartz windows were adapted as combustor side walls to allow flow visualization.

The operation of the direct-connect facility required first establishing the airflow through the flow path. The heater igniter would then be fired to then proceed with the injection of the main fuel and oxygen replenishment. With successful ignition of the main flow, the heater igniter would be shut off and the scramjet main fuel line and igniter lines would open for a three second period used to gather all the data. The firing sequence of the gas lines and the ignition systems was controlled using a NI cRIO-9022 with a custom made LabView interface.

The use of combustion preheat to simulate the high enthalpy flow conditions entering a scramjet combustor in flight has well known limitations, the most important one being the failure to match the chemical and thermodynamic properties of natural air[19]. This work placed less emphasis on the effects of using vitiated air with oxygen replenishment on the combustion kinetics and focused more on understanding the impact of using the mixing enhancement fin on the combustion characteristics.

B. Injection Conditions

Gaseous hydrogen was the fuel of choice for the experiments as it is considered a strong candidate for scramjet propulsion systems[20]. Five different combustor equivalence ratios (Φ_{comb}) were tested using room temperature fuel with each injection configuration. Fuel flow rates were determined using pressure measurements upstream of choked O'Keefe precision orifices recorded using an NI cDAQ-9188 system. These fuel pressures were calculated and preset before running the experiments given a target equivalence ratio. With the recorded gas flow rates after the experiments and by assuming complete combustion in the vitiated heater, an actual scramjet equivalence ratio was determined using the equation below:

$$\Phi_{comb} = \frac{\dot{m}_{H2} / \dot{m}_{O2,actual}}{\dot{m}_{H2} / \dot{m}_{O2,stoic}} = \frac{\dot{m}_{O2,stoic}}{\dot{m}_{O2,actual}} \quad (1)$$

The use of an igniter was required for the scramjet tests after combustion ignition failure in a set of preliminary experiments[‡]. The igniter operation used stoichiometric H_2/O_2 products for all the cases studied to ensure no additional fuel was injected into the test section. In the range of fuel flow conditions tested, the flames in the fin-guided configuration were not steady enough to self-sustain unless the igniter was left on. As a result, direct comparison between the two cases required leaving the igniter on while testing the various fuel injection conditions. Table 3 summarizes the actual test conditions for two sample sets of experiments that correspond to the pressure measurements and schlieren results shown in the following sections. The average heater stagnation pressure and temperature values recorded for each set of tests is included also.

[‡] The absence of combustion was likely due to the long ignition delay time associated with ~300 K hydrogen injection and the short combustor residence time.

Table 3. Sample experimental test conditions for one set of baseline (B) or fin-guided (F) injection tests.

Case	Vitiated Heater			Scramjet			
	P0 ±0.01 *atm*	**T0** ±15.1 *K*	$\dot{m}_{vit\ air}$ ±1.2 *gm/s*	$m_{H2,ign}$ *gm/s*	Φ_{ign}	$m_{H2,comb}$ *gm/s*	Φ_{comb}
B00	6.67	1142	87.4	0.00	0.00	0.00	0.00
B04				0.06	1.01	0.11	0.04
B08				0.06	1.01	0.21	0.08
B12				0.06	1.01	0.32	0.12
B15				0.06	1.01	0.42	0.15
B18				0.06	1.02	0.52	0.18
F00	6.69	1105	88.1	0.00	0.00	0.00	0.00
F04				0.06	1.01	0.10	0.04
F09				0.06	1.01	0.23	0.09
F11				0.06	1.01	0.31	0.11
F15				0.06	1.01	0.42	0.15
F19				0.06	0.99	0.53	0.19

C. Flow Diagnostics

Key to this work was monitoring combustor pressure rise and obtaining corresponding flow visualizations using both injection configurations. Static pressure distributions were therefore obtained along the upper wall of the isolator and combustor sections using a Scanivalve DSA-3217 Digital Sensor Array. This sensor array consisted of temperature compensated piezoresistive pressure sensors with a pneumatic calibration valve and a range of 0-1.5MPa. Pressure taps lined along the supersonic duct centerline and spaced *1H* apart were installed as shown in Figure 2 to obtain measurements at a maximum of 16 locations per run with the available channels. A total of 26 locations were probed for each equivalence ratio tested by running two consecutive tests and shifting the measurement locations. Pressure readings were obtained at a 25 Hz rate and were sent via a TCP/IP connection to a desktop computer and into a LabView virtual control panel. This interface allowed monitoring the 16 channels and DSA settings as well as writing of the data to a text file to be read by post-processing software.

Schileren and *OH** chemiluminescence imaging were the main flow visualization techniques used to study the reacting flow and characterize its behavior for the two injection methods tested. A conventional Z-schlieren arrangement was used to obtain side profile density gradient images of a portion of the isolator and combustor sections shown in Figure 2 (yellow). A high speed NR3-S1 camera was used with an LS-1130 Flash Pac light source, two spherical *f/10* mirrors, and a horizontal knife edge for this setup. The images were recorded a rate of 800 Hz in order to synchronize the imaging with the pressure measurements recorded every 32 frames. The exposure of the images captured was determined by the pulse duration of the flash pack which was 3-10μs long. A Motion Studio computer software was used to control the camera as well as to record, access, and save the images.

The chemiluminescence de-excitation of the *OH** radical was used to complement the schlieren images obtained. The *OH** signal captured was used as an optical marker of heat release occurring through the exothermic $H + O + M \rightarrow OH^* + M$ reaction in the combustor. A Dicam Pro ICCD camera with an ultraviolet lens and a 308 nm band pass filter was used to collect the *OH** chemiluminescence radiation at a frequency of 5 Hz. The images had a long 150 ms exposure and therefore were a time averaged representation of the $OH^* \rightarrow OH + h\upsilon$ decay signal.

The NI CompactRIO-9022 controller responsible for the gas line sequencing and firing of the heater and scramjet ignition systems was also used to trigger the data acquisition (NI CompactDAQ-9188, DSA 3217 Scanivalve, and NR3-S1 or Dicam Pro ICCD cameras). This unified control system arrangement allowed triggering the experiment simultaneously with the data acquisition but also synchronizing the pressure measurements and schlieren visualizations.

III. Results and Discussion

A. Combustion Mode

The static pressure distributions obtained along the top wall centerline of the isolator and combustor are presented in Figure 4 for both baseline and fin-guided injection. The measurements presented were normalized by the heater exit stagnation pressure and are shown as a function of axial distance *x* normalized by combustor height, *H*. In comparison to the no injection case, the baseline measurements obtained *with* fuel injection show a clear rise in combustor pressure observed in the cavity near region. Pressure increased as a result of fuel mass addition and the heat release generated by its combustion. As more fuel was injected, the wall pressure rise increased with a similar profile. This progressive pressure rise seen with the baseline contrasted the pressure distributions obtained using fin-guided injection in the Φ_{comb} = 0.04 - 0.19 range tested. When using the fin, a clear discontinuity between the lowest three and highest two fueling conditions was observed.

To aid the interpretation of the pressure results and gain physical insight into the combustion flowfields, Figure 5 shows a set of sample instantaneous schlieren images of the reacting flow for the injection conditions tested. From these results, the baseline showed a flame located in the cavity for all the fuel injection cases studied. However, there were substantial differences in the shock flowfields observed. For the Φ_{comb} = 0.04 - 0.08 conditions, the flow upstream of the injection point was undisturbed and remained supersonic, as indicated by the visible jet-induced shocks for both fuel and igniter jets. Similarly, the oblique shocks seen downstream of the injection point and over the flame, suggest supersonic heat addition for these two injection conditions. At higher fueling rates, the increasing adverse pressure gradient in the cavity region due to the increased fuel flux and heat addition, slowed down the flow and forced the combustor pressure to adjust through a set of oblique and normal shocks clearly seen for the Φ_{comb} = 0.12 - 0.18 images. This result was consistent with the behavior of the corresponding pressure traces which showed increasing combustor peak pressures and an upstream motion of the pressure rise with increasing equivalence ratio.

While the baseline images showed the evolution of a thermal choking event with increasing fuel flow rate, the fin-guided results in Figure 5 showed two disparate combustion flowfields that coincide with the two distinct behaviors seen in the pressure traces presented in Figure 4. For the lowest three fueling conditions, the images showed fin induced and igniter induced shocks as well as flames with shock-like structures beyond the cavity, suggesting supersonic flow in that part of the duct. For the highest two fueling conditions, conversely, the flame was captured by the cavity in a similar way as the baseline and the combustor operated in a thermally choked mode.

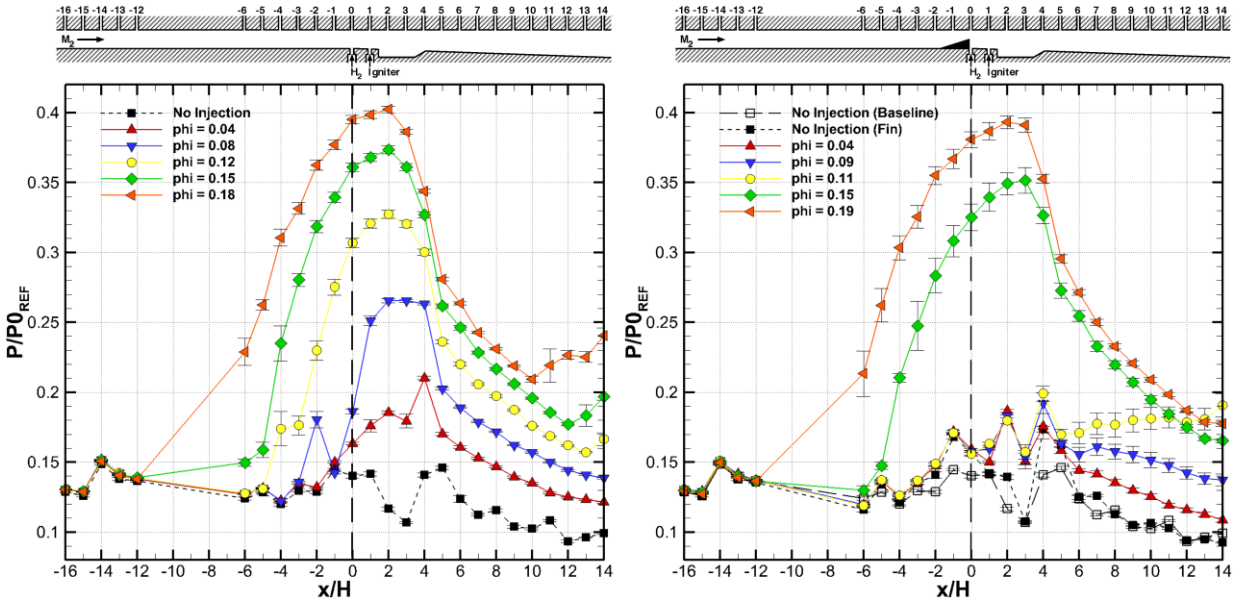

Figure 4. Baseline *(left)* and fin-guided *(right)* normalized pressure distributions as a function of combustor equivalence ratio. The reference pressure used for normalization corresponds to the heater exit stagnation pressure, $P0_{REF} = P0_{\infty}$.

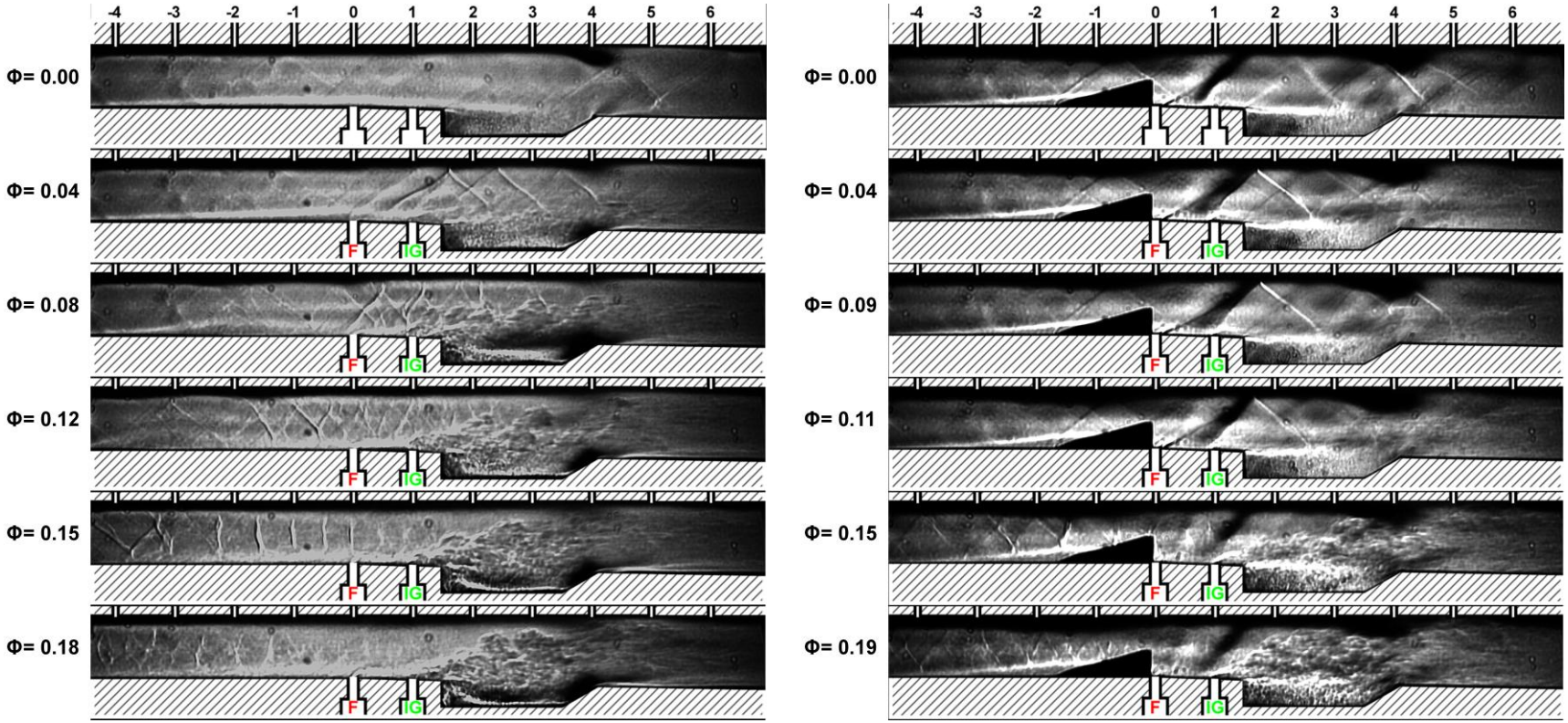

Figure 5. Sample schlieren images for baseline *(left)* and fin-guided *(right)* hydrogen fuel injection for varying fuel injection conditions. Two no-injection images (Φ_{comb} = 0.00) are shown as a reference for comparison with the fuel injection cases. Flow direction is left to right in all the images. Fuel injection (F) and igniter (IG) locations are highlighted. The use of a horizontal knife edge enables the visualization of vertical density gradients in the images.

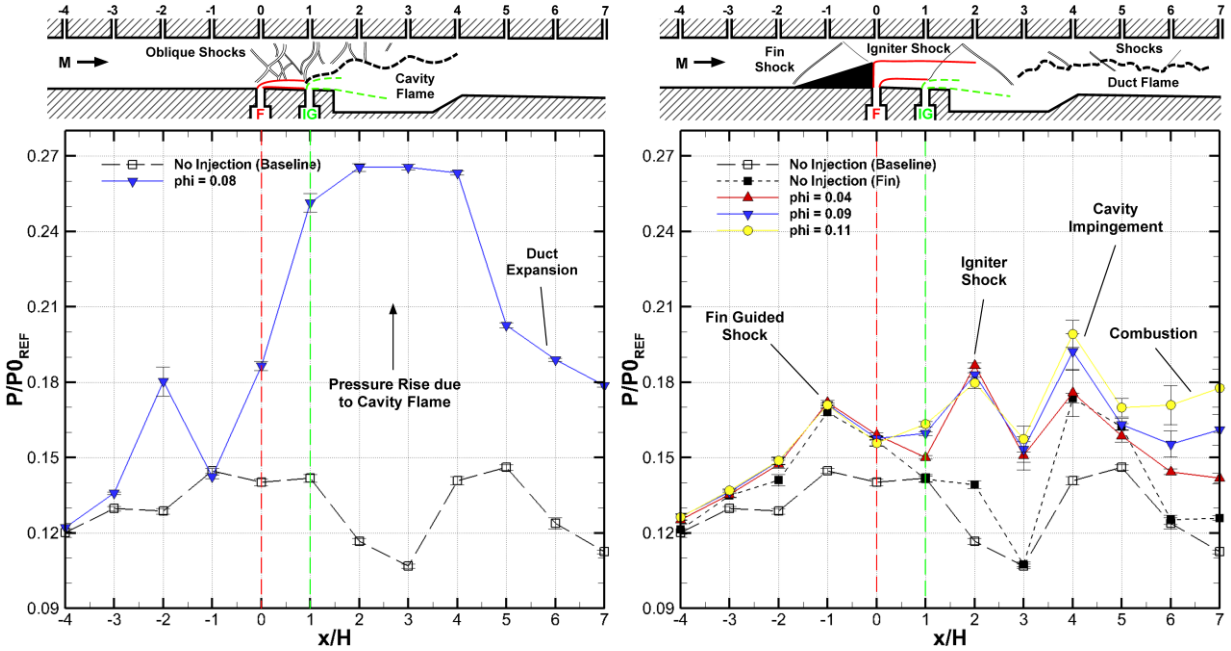

Figure 6. Effect of flame location on combustor pressure measurements in the injection near field, baseline *(left)*, fin-guided *(right)*.

For the fuel injection cases where the flow was not thermally choked (Φ_{comb} = 0.04 - 0.8 for the baseline and Φ_{comb} = 0.04 - 0.11 for the fin), the location of the flame and the shock structures seen in the schlieren images explain the substantial differences in the wall pressure distributions of the two injection configurations. Taking the Φ_{comb} = 0.08 case as an example for the baseline, the cavity-anchored flame increased the pressure locally generating some oblique shocks in the flow. Downstream of the cavity the flow expanded and the pressure dropped in the diverging duct as seen in Figure 6. With fin-guided injection, the lowest three fuel injection conditions had a similar pressure distribution up to the *x/H* = 5 location, characterized by three comparable pressure peaks caused by the fin-induced shock, the igniter induced shock, and the effect of the cavity. Downstream of the *x/H* = 5 location, the pressure traces diverged and a pressure rise was observed for the Φ_{comb} = 0.09 - 0.11 cases in the expanding duct. This result suggests that the heat addition process occurred downstream of the cavity, which agrees with the location of the flame observed in the images.

B. Combustion Characteristics

The chemiluminescence emission generated by the de-excitation of the *OH** radical was captured to map the reaction zones and complement the previously described schlieren and combustor pressure results. Figure 7 contains two sample *OH** images overlaid onto two sample schlieren images corresponding to approximately the same equivalence ratio condition (Φ_{comb} = 0.11-0.12). The chemiluminescence images used in these figures were processed following the procedure by Laurence[21] using Matlab to remove the green and blue components of every pixel and so the *OH** signal presented appears red. The intensity of the schlieren images was also reduced in order to enable the visualization of the added *OH** signal information.

Although the *OH** images presented are essentially an average representation of the chemiluminescence emission due to their long exposure (150ms compared to the 3-10μs schlieren exposure), this overlay was still useful to qualitatively verify the flame observations in the schlieren visualizations. The processed overlays clearly confirm that most of the reaction for the baseline was concentrated inside the cavity. When using the fin, some *OH** is visible in the expansion section of the duct matching the location of the flame seen in the schlieren.

The *OH** chemiluminescence images obtained also provided additional flame information not captured by the instantaneous density gradient images. Figure 8 compares the *OH** signal intensity occurring for both injection configurations as a function of equivalence ratio. These results were obtained by computing an average *OH** image during the steady state portion of injection (same time window as pressure and schlieren) and then normalizing the

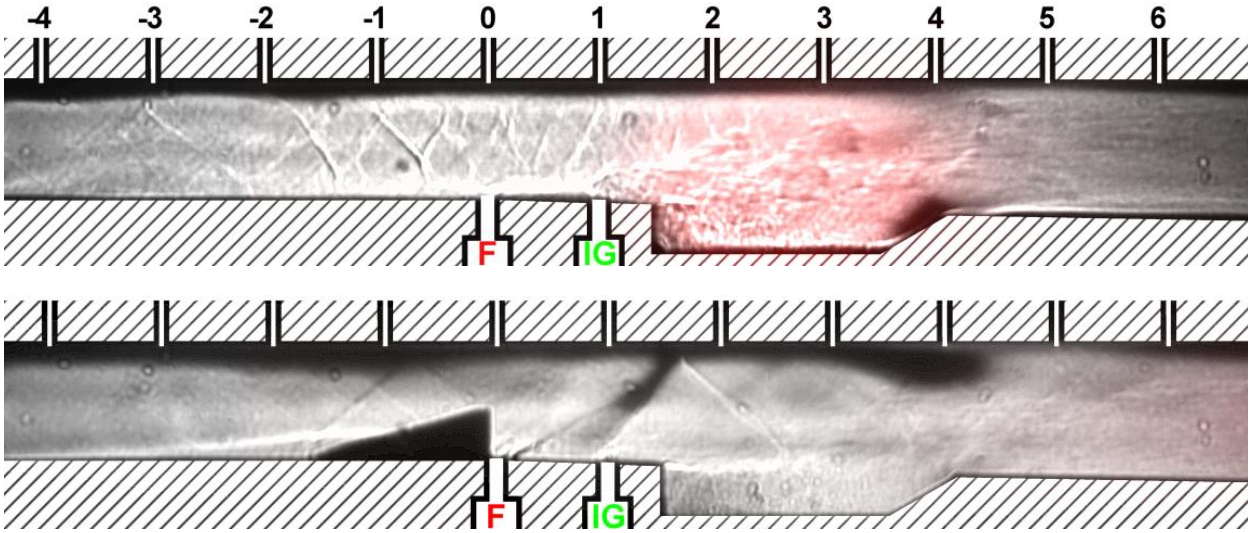

Figure 7. Baseline (top) and fin-guided (bottom) overlay of OH* chemiluminescence (red) on instantaneous schlieren images (gray).

result with a background (no injection) image. A non-linear intensity scale with 20 different bins was used to color the *OH** signal based on the lowest and highest normalized intensity values from the entire set of images (baseline and fin-guided).

The intensity contours clearly show how with fin-guided injection most of the reaction occurred downstream of the cavity and over a longer distance compared to the baseline. The *OH** intensity distribution was also significantly different between both configurations for the lowest three fueling cases. While the baseline shows a sizeable high intensity core with relatively thin low intensity rings, the *OH** signal seen when using the fin had a small high intensity core surrounded by a long, oblong low intensity zone. Besides achieving a more distributed heat release through the combustor with the fin, the difference in intensity distribution has one important additional implication. Since the highest *OH** intensity was seen in the core of the flow, most of the exothermic $H + O + M \rightarrow OH + M$ reaction occurred away from the bottom combustor wall. By displacing the location of the reaction then, heat transfer losses to the structure can be reduced, which in turn is beneficial to minimize the combustor *T0* losses.

Another particular feature of the results shown in these two figures is the stretching of the chemiluminescence regions with increasing fuel flow rate. For the baseline, the reaction expanded downstream as the excess fuel not consumed in the cavity escaped the flame holder. From the fin-guided contours, the reaction zone stretched initially downstream for a $\Phi_{comb} = 0.08$ and then propagated upstream into the cavity for the $\Phi_{comb} = 0.12$ condition. Since each of the *OH** intensity contours shown here corresponds to an average image obtained for the duration of the injection process, this third fueling case suggests that this condition is at the boundary between scramjet and ramjet operation for fin-guided fuel injection. Further tests using the fin for the $\Phi_{comb} = 0.12$ condition showed that after initially operating in scramjet mode, a mode transition did occur with time. Although understanding the mechanism that triggered the transition was beyond the scope of the experiments, one possible explanation for this behavior could be a decrease in heat transfer to the combustor walls with time and the consequent increase in heat addition to the flow. Finally, and as seen previously with the pressure and schlieren results, for the fully thermally choked conditions (highest two fueling cases), the intensity contours are very similar for both injection configurations.

The chemiluminescence images obtained were also used to determine a reaction length as a function of equivalence ratio. To do so, raw images gathered during the injection steady state were used to once again obtain an average *OH** image and then calculate its average normalized intensity as a function of *x/H*. Figure 9 highlights the region of the combustor analyzed with Matlab to obtain the intensity curves *I(x/H)* and summarizes the results for both injection configurations. From these curves, the maximum *OH** location was determined and used as a reference to define flame length based on the full width at half-maximum (FWHM) of each distribution.

Figures 10 and 11 map the locations of peak *OH** intensity with the corresponding flame length values obtained and show a schematic of the flowfield seen at three selected fueling conditions that help explain the combustion process with each injector. The baseline results presented in Figure 10 show how the maximum *OH** intensity was found very close to the *x/H* = 3 location (inside the cavity as expected) for all injection cases tested. The flame

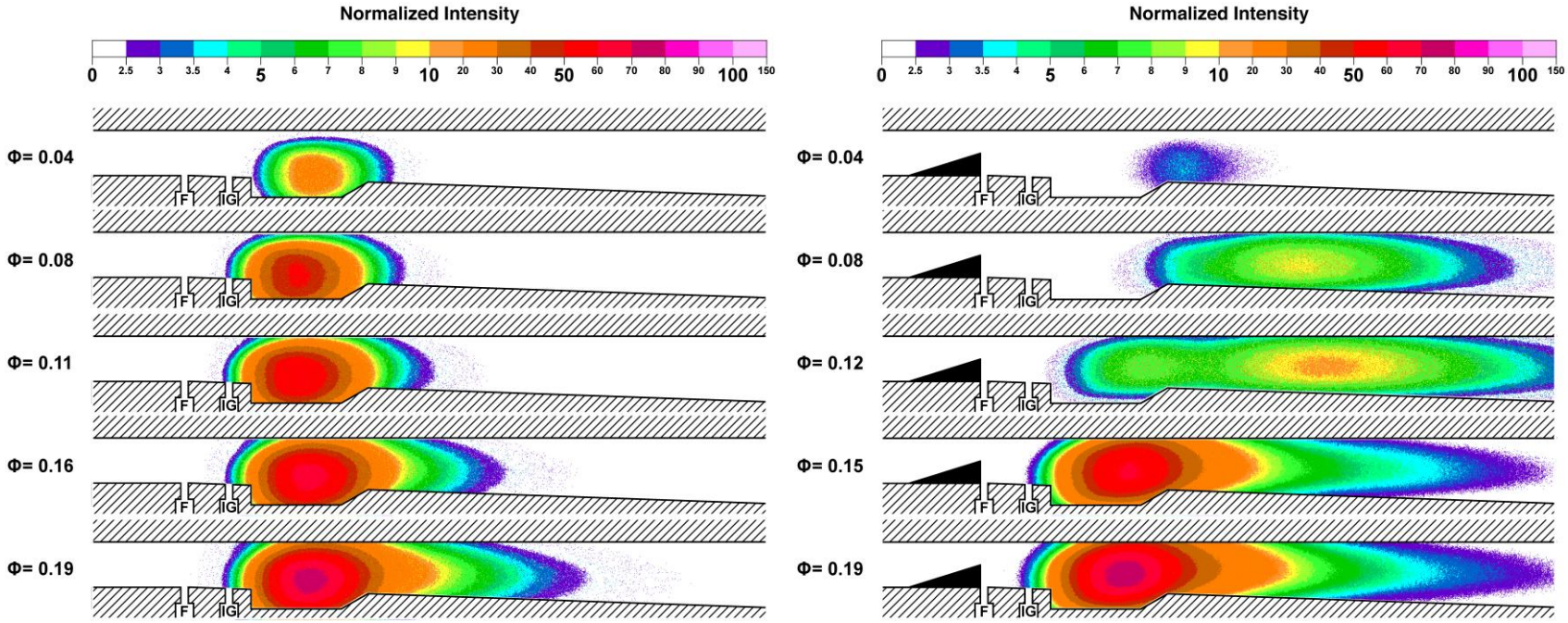

Figure 8. Normalized OH* intensity contours for baseline *(left)* and fin-guided injection *(right)*.

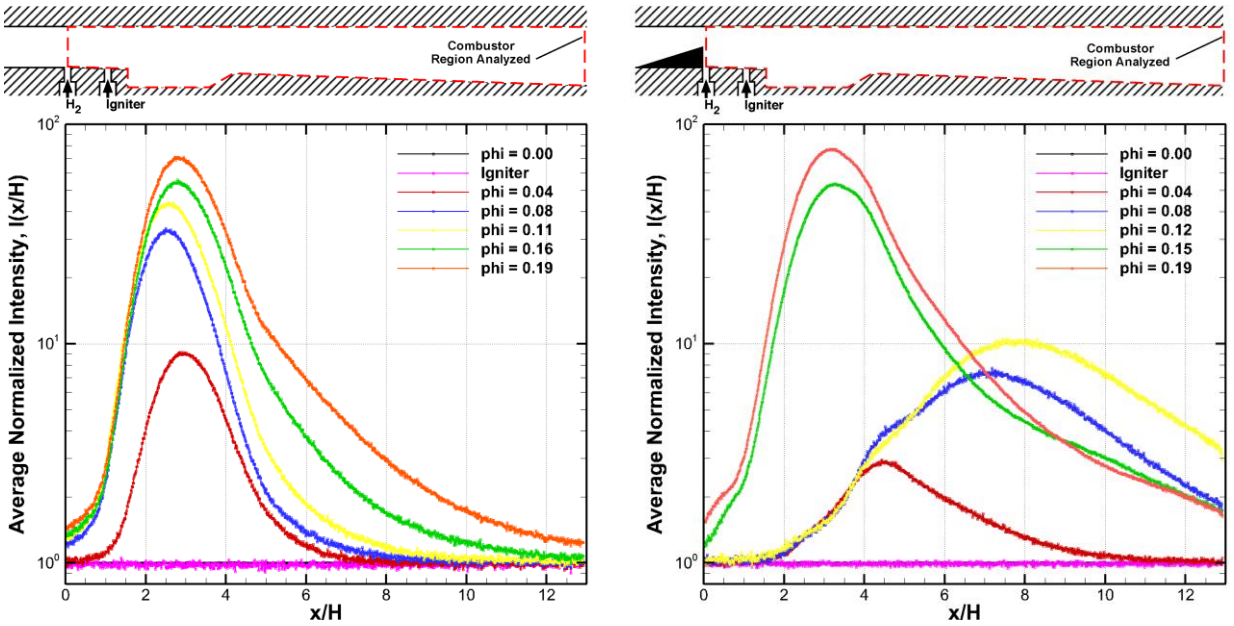

Figure 9. Average combustor OH* chemiluminescence intensity results as a function of combustor axial location for baseline *(left)* and fin-guided injection *(right)*. The peak intensity of these distributions and the full width at half maximum were used to quantify flame length.

lengths obtained averaged two duct heights (2*H*) and showed a slight widening effect with increasing fuel mass flow rate. When using the fin, substantial differences were seen in the peak reaction locations as shown in Figure 11 and as hinted earlier in the *OH** intensity contours. For the lowest three fuel injection cases (Φ_{comb} = 0.04 - 0.12), the peak *OH** chemiluminescence location shifted downstream and there was a significant increase in the length of the reaction zone (~ 4.5*H* – 5.6*H*).

The physical mechanism responsible of these contrasting *OH** results and the previously discussed differences in the pressure distributions and schlieren visualizations was the jet penetration allowed by each injector. As seen in the flow schematics in Figure 10 (A-C), for all the injection conditions, low penetration in the baseline allowed the fuel jet to impinge on the igniter flow, mix in the cavity shear layer, and become more vigorous with increasing fuel rate. Fuel was therefore consumed in a well stirred reaction zone that anchored the flame. Initially the heat addition process was supersonic as seen in Figure 10 (A) but with additional fuel injection, the reaction intensified as shown in the *OH** results, increasing the heat release and the combustor pressure. At some point prior to a Φ_{comb} = 0.12, a scramjet to ramjet combustion mode transition occurred due to thermal choking as observed in the sample schlieren images.

Increased fuel penetration when using the fin enabled most of the fuel to be delivered into the faster moving core of the combustor as shown schematically in Figure 11 (D-F). As a result, the fuel was lifted away from the bottom combustor wall and traveled beyond the cavity into the expanding duct, where supersonic combustion occurred in a strained reaction zone for the Φ_{comb} = 0.04 - 0.11 cases. With the fin, ignition occurred just downstream of the cavity where the igniter flow and the fast moving fuel interacted. The cavity in that sense played an important role in the ignition of the fuel-air mixture due to the impingement of the hot igniter combustion products on its angled end. For the Φ_{comb} = 0.04 condition, the reaction was weak and relatively short due to the small amount of fuel available, but as the equivalence ratio increased, a larger amount of fuel reached further into the expanding duct as illustrated in Figure 11 (E). This caused the reaction zone for the Φ_{comb} = 0.08 - 0.11 cases to stretch as demonstrated by the distributed *OH** chemiluminescence intensity and the increased flame length.

Finally and as mentioned before, the Φ_{comb} = 0.12 condition was a special case because it stood out as the transition point between supersonic and subsonic combustion for fin-guided injection. Although an unsteady condition, the peak *OH** location and the rising pressure profile in the expanding duct (Figure 4) for this case showed that the heat addition was possible in scramjet mode. The importance of this result is demonstrating that the fin allowed scramjet operation for a higher fueling condition compared to the baseline, which visibly choked beyond a Φ_{comb} = 0.8 as seen in the schlieren.

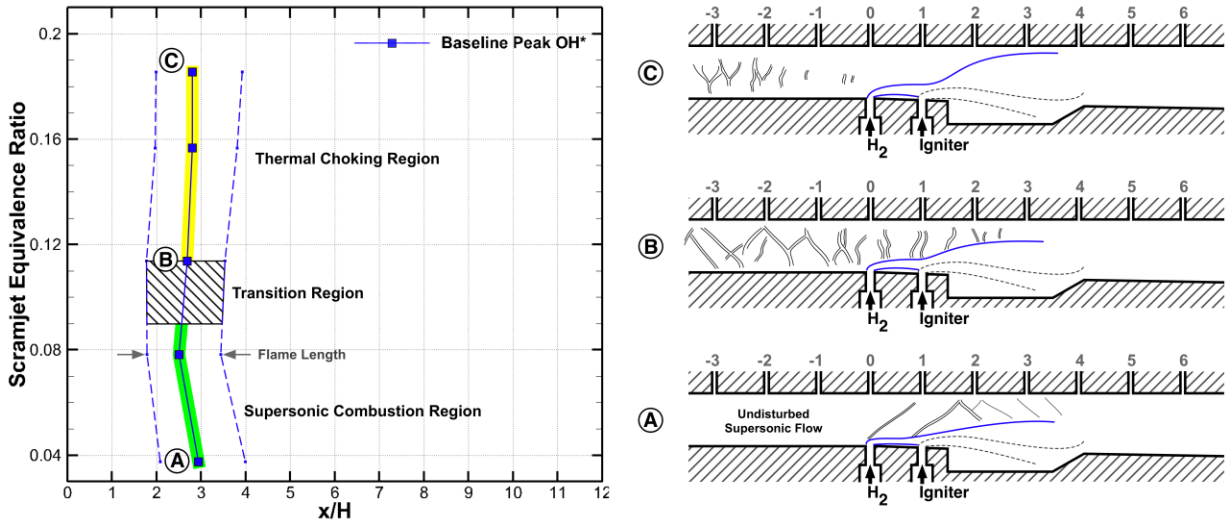

Figure 10. Locus of peak *OH locations within the combustor for baseline injection. The corresponding flame length as a function of equivalence ratio is represented by the distance between the dashed lines on the left and right of the peak *OH** locations. A schematic of the flowfield at three selected fuel injection conditions is also shown.**

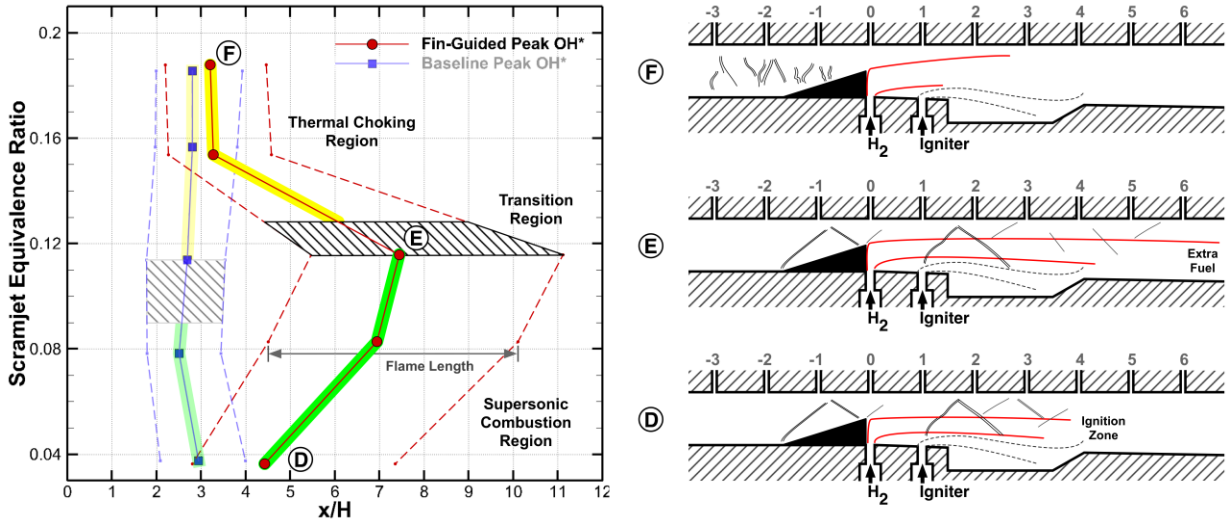

Figure 11. Locus of peak *OH locations within the combustor for fin-guided fuel injection with corresponding flame length as a function of equivalence ratio. Flowfield schematics also shown.**

IV. Summary and Concluding Remarks

An experimental investigation was performed to examine and compare the combustion characteristics of a dual mode scramjet combustor using normal fuel injection with and without a jet-guiding fin. A range of combustor equivalence ratios between Φ_{comb} = 0.04 - 0.19 were studied using hydrogen as the main fuel with both injection configurations. The laboratory-scale tests used a vitiated heater to match the total enthalpy of the flow expected for a Mach 4.6 flight condition. Fuel injection was done downstream of an isolator section with an inlet Mach 2 flow. A bottom wall igniter and cavity were used throughout the experiments for ignition and flameholding, respectively.

Dual mode combustion operation was observed with both injection configurations for the range of hydrogen fueling conditions tested, but the critical equivalence ratio for the scramjet to ramjet transition was different between injectors. Schlieren visualizations and static pressure measurements indicated that while scramjet mode operation occurred up to a $\Phi_{comb} = 0.08$ with the baseline, fin-guided injection extended that range up to a $\Phi_{comb} = 0.12$. For the $\Phi_{comb} = 0.16 - 0.19$ cases tested however, both injection configurations operated in a very similar thermally choked mode.

Up to $\Phi_{comb} = 0.12$, clear changes in the flame location, length, and reaction intensity distribution occurred when using the fin in comparison to the baseline. Processed *OH** chemiluminescence results showed that without the fin, the reaction zone was confined to the cavity, had an average ~2*H* length, and was characterized for having a large high intensity core. With the fin, the reaction zone was located in the diverging duct, had a ~4.5-5.6*H* length depending on the fuel rate, and showed a significantly more spread out intensity distribution.

Jet penetration played a fundamental role in determining the reaction zone characteristics and the combustor operating mode for each injection method up to a $\Phi_{comb} = 0.12$. Low fuel penetration with the baseline favored fuel delivery into the cavity, which concentrated the heat release. This caused a local steep pressure rise that lead to a thermally choked combustion mode operation beyond $\Phi_{comb} = 0.08$. Increased fuel penetration when using the fin allowed most of the fuel to be delivered into the core flow and away from the cavity. As a result, the reaction zone was displaced downstream into the expanding duct, but also enabled a more distributed heat release with a lower pressure rise, extending the scramjet mode operation.

Some of the key findings of this investigation can be used to extrapolate possible implications of using fin-guided injection in a real system. Extending the supersonic mode operation can be advantageous for propulsion performance considerations if scramjet mode is preferred for the given flight condition. Distributing the exothermic reaction inside the combustor and displacing it away from its walls can be beneficial if it leads to a reduction in the structural thermal loads and a decrease in stagnation temperature losses. However, this must be evaluated against the requirement for a longer combustor and the weight penalty associated with it. Fin-guided injection also deprived the cavity of fuel, reducing its flameholding capability. Since the thin fin base cannot generate a recirculation zone strong enough to support adequate flameholding, flame stability concerns clearly constitute the main disadvantage of using this proposed injection scheme.

Acknowledgments

This work was supported by the Office of Naval Research under grant N000140711185 monitored by scientific officers Gabriel Roy and Clifford Bedford. The authors would also like to acknowledge the additional support for the development of the heater facility provided by NAVAIR under a task managed by David Barrett, and the support for personnel training, provided by the Air Force Office of Scientific Research under the UMD Center for Revitalization of the Hypersonic Testing and Evaluation Workforce program, managed by Michael Kendra.

References

[1]D. Bogdanoff, "Compressibility Effects in Turbulent Shear Layers," *AIAA Journal*, vol. 21, no. 6, pp. 926-927, 1983.

[2]N. Chinzei, G. Masuya, T. Komuro, A. Murakami and K. Kudou, "Spreading of two-stream supersonic turbuelnt mixing layers," *Physical Fluids*, vol. 29, no. 5, pp. 1345-1347, 1986.

[3]D. Papamoschou and A. Roshko, "The compressible turbulent shear layer: an experimental study," *Journal of Fluid Mechanics*, vol. 197, pp. 453-477, 1988.

[4]D. Papamoschou, "Structure of the compressible turbulent shear layer," in *AIAA Paper 89-0126*, January 1989.

[5]M. Gruber, A. Nejad, T. Chen and J. Dutton, "Compressibility Effects in Supersonic Transverse Injection Flowfields," *Physics of fluids*, vol. 9, no. 5, 1997.

[6]G. Elliot, M. Samimy and S. Arnette, "The characteristics and evolution of large-scale structures in compressible mixing layers," *Physics of Fluids*, vol. 7, no. 4, pp. 864-876, April 1995.

[7]N. Messersmith, J. Dutton and H. Krier, "Experimental investigation of large scale structures in compressible mixing layers," in *AIAA Paper 91-0244*, January 1991.

[8]N. Clemens and M. Mungal, "Two and three dimensional effects in the supersonic mixing layer," *AIAA Journal*, vol. 30, no. 4, pp. 973-981, April 1992.

[9]K. Yu and K. Schadow, "Role of Large Coherent Structures in Turbulent Compressible Mixing," *Experimental Thermal and Fluid Science,* vol. 14, pp. 75-84, 1997.

[10]E. Gutmark, K. Schadow and K. Yu, "Mixing Enhancement in Supersonic Free Shear Flows," *Anual Review of Fluid Mechanics,* vol. 27, pp. 375-417, 1995.

[11]E. Gutmark, K. Schadow and K. Wilson, "Subsonic and supersonic combustion using noncircular injectors," *Journal of Propulsion and Power,* vol. 7, no. 2, pp. 240-249, April 1991.

[12]K. Yu, K. Schadow, K. Kraeutle and E. Gutmark, "Supersonic Flow Mixing and Combustion Using Ramp Nozzles," *Journal of Propulsion and Power,* vol. 11, no. 6, November-December 1995.

[13]K. Yu, K. Wilson and K. Schadow, "Effect of Flame-Holding Cavities on Supersonic Combustion Performance," *Journal of Propulsion and Power,* vol. 17, no. 6, pp. 1287-1295, 2001.

[14]W. VanLerberghe, J. Santiago, J. Dutton and R. Lucht, "Mixing of a sonic transverse jet injected into a supersonic flow," *AIAA Journal,* vol. 38, no. 3, pp. 470-479, March 2000.

[15]W. VanLerberghe, J. Dutton, R. Lucht and L. Yuen, "Penetration and mixing studies of a sonic transverse jet injected into a Mach 1.6 crossflow," in *25th AIAA Fluid Dynamics Conference, AIAA Paper 94-2246*, Colorado Springs, CO, 1994.

[16]M. Gruber, A. Nejad, T. Chen and J. Dutton, "Mixing and penetration studies of sonic jets in a Mach 2 freestream," *Journal of Propulsion and Power,* vol. 11, no. 2, pp. 315-323, March- April 1995.

[17]A. Ben-Yakar, M. Mungal and R. Hanson, "Time evolution and mixing characteristics of hydrogen and ethylene transverse jets in supersonic crossflows," *Physics of Fluids,* vol. 18, no. 2, 2006.

[18]C. Aguilera, B. Pang, A. Ghosh, A. Winkelmann, A. Gupta and K. Yu, "Supersonic Mixing Enhancement and Optimization using Fin-Guided Fuel Injection," in *48th AIAA Aerospace Sciences Meeting, AIAA 2010-1526*, Orlando, FL, 2010.

[19]C. Goyne, J. McDaniel Jr., R. Krauss and W. Whitehurst, "Test Gas Vitiation Effects in a Dual Mode Scramjet Combustor," *Journal of Propulsion and Power,* vol. 23, no. 3, pp. 559-565, 2007.

[20]C. Segal, The Scramjet Engine: Processes and Characteristics, Cambridge University Press, 2009.

[21]S. Laurence, J. Martinez-Schramm, S. Karl and K. Hannemann, "An Investigation of Steady and Unsteady Combustion Phenomena in the Hyshot II Combustor," 2011.